LBL-33149
UC-403

Lawrence Berkeley Laboratory

UNIVERSITY OF CALIFORNIA

EARTH SCIENCES DIVISION

Presented at the 1993 SPE Symposium on Reservoir Simulation, New Orleans, LA, February 28–March 3, 1993, and to be published in the Proceedings

The Transformational Decomposition (TD) Method for Compressible Fluid Flow Simulations

G.J. Moridis and D.A. McVay

November 1992

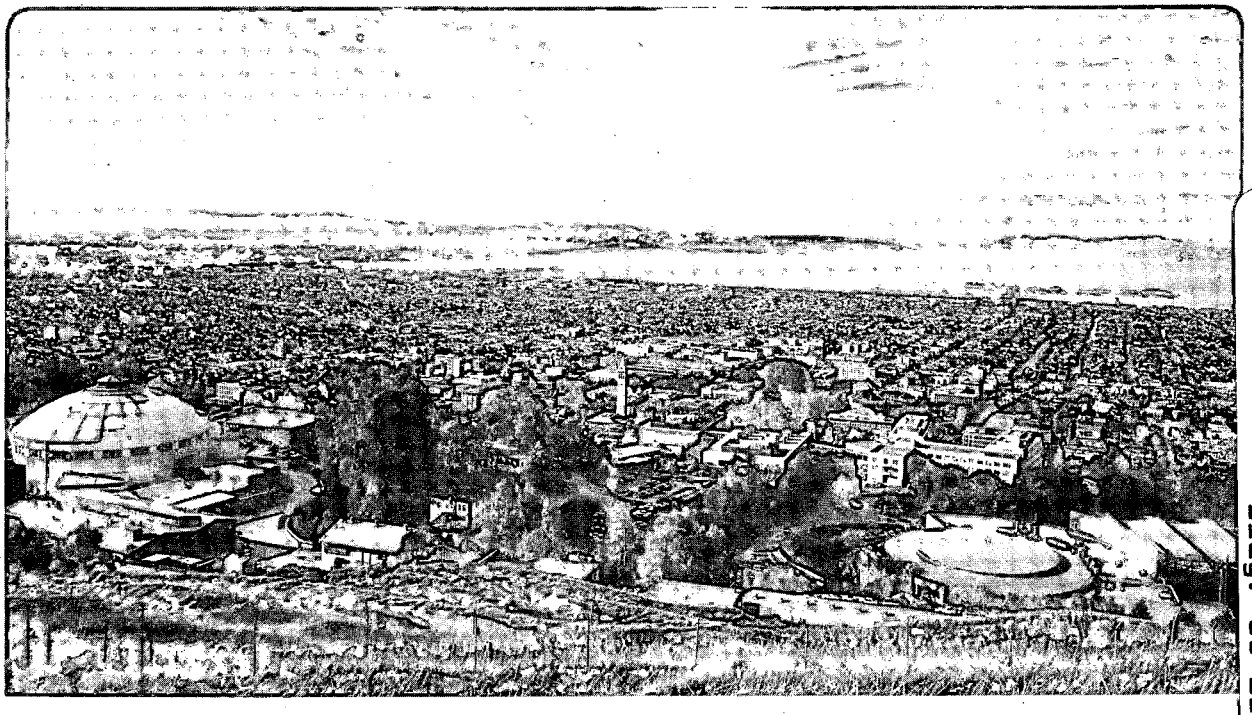

REFERENCE COPY
Does Not
Circulate
Bldg. 50 Library.
LBL-33149
Copy 1

Prepared for the U.S. Department of Energy under Contract Number DE-AC03-76SF00098

DISCLAIMER

This document was prepared as an account of work sponsored by the United States Government. Neither the United States Government nor any agency thereof, nor The Regents of the University of California, nor any of their employees, makes any warranty, express or implied, or assumes any legal liability or responsibility for the accuracy, completeness, or usefulness of any information, apparatus, product, or process disclosed, or represents that its use would not infringe privately owned rights. Reference herein to any specific commercial product, process, or service by its trade name, trademark, manufacturer, or otherwise, does not necessarily constitute or imply its endorsement, recommendation, or favoring by the United States Government or any agency thereof, or The Regents of the University of California. The views and opinions of authors expressed herein do not necessarily state or reflect those of the United States Government or any agency thereof or The Regents of the University of California and shall not be used for advertising or product endorsement purposes.

Lawrence Berkeley Laboratory is an equal opportunity employer.

This publication has been reproduced from the best available copy

DISCLAIMER

This document was prepared as an account of work sponsored by the United States Government. While this document is believed to contain correct information, neither the United States Government nor any agency thereof, nor the Regents of the University of California, nor any of their employees, makes any warranty, express or implied, or assumes any legal responsibility for the accuracy, completeness, or usefulness of any information, apparatus, product, or process disclosed, or represents that its use would not infringe privately owned rights. Reference herein to any specific commercial product, process, or service by its trade name, trademark, manufacturer, or otherwise, does not necessarily constitute or imply its endorsement, recommendation, or favoring by the United States Government or any agency thereof, or the Regents of the University of California. The views and opinions of authors expressed herein do not necessarily state or reflect those of the United States Government or any agency thereof or the Regents of the University of California.

LBL-33149

The Transformational Decomposition (TD) Method for Compressible Fluid Flow Simulations

G. J. Moridis[*] *and D. A. McVay*[†]

[*]Earth Sciences Division
Lawrence Berkeley Laboratory
University of California
Berkeley, California 94720

[†]S.A. Holditch & Assoc.
700 Southwest Parkway, Suite 200
College Station, Texas 77840

November 1992

This work was supported by the Director, Office of Energy Research, Office of Basic Energy Sciences, under U.S. Department of Energy Contract No. DE-AC03-76SF00098.

SPE 25264

The Transformational Decomposition (TD) Method for Compressible Fluid Flow Simulations

G.J. Moridis, SPE, Lawrence Berkeley Laboratory, and **D.A. McVay,** SPE, S.A. Holditch & Assoc.

Abstract

A new method, the Transformational Decomposition (TD) method, is developed for the solution of the Partial Differential Equations (PDE's) of single-phase, compressible liquid flow through porous media. The major advantage of the TD method is that it eliminates the need for time discretization, and significantly reduces space discretization, yielding a solution semi-analytical in time and analytical in space. There are two stages in the TD method: a Decomposition stage and a Reconstitution stage. In the Decomposition stage the original PDE is decomposed by using a Laplace transform for time, and successive levels of finite integral transforms for space. Each level of finite integral transform eliminates one active dimension, until a small set of algebraic equations remain. The original PDE is thus decomposed into much simpler algebraic equations, for which solutions are obtained in the transformed space. In the Reconstitution stage, solutions in space and time are obtained by applying succesive levels of inverse transforms. In contrast to traditional numerical techniques, the TD method requires no discretization of time and only a very coarse space discretization for stability and accuracy. The TD method is tested against results from one- and two-dimensional test cases obtained from a standard Finite Difference (FD) simulator, as well as from analytical models. The TD method may significantly reduce the computer memory requirements because discretization in time is not needed, and a very coarse grid - corresponding to inhomogeneous regions - suffices for the space discretization. Execution times may be substantially reduced because smaller matrices are inverted in the TD method, and solutions are obtained at the desired points in space and time only, while in standard numerical methods solutions are necessary at all of the points of the discretized time and space domains.

Introduction

In transient flow through porous media, the Partial Differential Equation (PDE) to be solved is obtained by combining appropriate forms of Darcy's Law and the equation of mass conservation, yielding:

$$\nabla \cdot \left[k \frac{\rho}{\mu} \left(\nabla p - \rho g \nabla z \right) \right] = \frac{\partial}{\partial t} (\rho \phi) + \tilde{q}. \qquad (1)$$

Eq. 1 is generally nonlinear, and in all but the simplest problems is solved numerically. The basic concept of any numerical method is the substitution of a set of algebraic equations for the original PDE. Instead of solving for the continuous smooth function $p(x, y, z, t)$, the space domain (x, y, z) is subdivided in N_D subdomains, and the time t is discretized in N_T timesteps; N_T sets of approximations $\tilde{p}$ of the solution are obtained at the N_D predetermined points in space. A PDE problem with a continuous smooth solution surface is thus reduced to a set of algebraic equations, which are easier to solve and provide a solution arithmetically "close" to the true solution, from which they differ by the truncation error $e = p - \tilde{p}$.

Despite their power and flexibility, numerical solutions have some serious drawbacks. Minimization of the error introduced by the numerical approximation of the spatial derivatives in the PDE's dictates the discretization of the space domain into a large number of subdomains at all of which solutions must be obtained (whether desired or not). This increases the execution time requirements and requires a large amount of computer memory, especially when direct matrix solvers are used. The approximation of the time derivatives in the PDE's is one of the most important sources of instability and error. Accuracy and stability considerations necessitate a large number of small timesteps between observation times; solutions must be obtained at all these intermediate times, increasing the execu-

tion times and the roundoff errors. The problem of restriction on the size of Δt is exacerbated by the nonlinearity of the PDE, which is caused by the pressure dependence of the liquid density and the formation porosity. This necessitates even shorter timesteps, dictates internal iterations within each timestep until a convergence criterion is met, and adds significantly to the computational load.

The Transformational Decomposition (TD) method is a new method which addresses the aforementioned shortcomings of traditional numerical techniques. The TD method was first applied to the solution of the diffusion-type (parabolic) PDE of incompressible flow through porous media[1]. It is based on successive integral transforms, and is an extension of the approach used by Goode and Thambynayagam[2] in the analysis of pressure response of horizontal wells. The major advantage of the TD method is that it requires no time discretization and a very coarse space discretization to yield an accurate, stable solution which is semi-analytical in time and analytical in space. In this paper, the TD method is formulated to address the problem of slightly compressible, single-phase liquid flow through porous media. The mathematical basis of the method is developed, and its performance is evaluated against analytical solutions and standard FD models.

The Transformational Decomposition (TD) Method

If gravity is negelected and porosity is considered constant, then Eq. 1 becomes

$$\nabla \cdot (k \nabla p) = \phi \, \mu \, C_L \, \frac{\partial p}{\partial t} + q. \tag{2}$$

A more robust approach is provided by the formulation of Moridis *et al.*[3] which maintains the generality but alleviates the nonlinearity in Eq. 1, resulting in

$$\nabla \cdot \left[\lambda \nabla r - \eta \left(1 + 2r + r^2\right)\right] = C_T \, \frac{\partial r}{\partial t} + q, \tag{3}$$

where $\lambda = k/(\mu C_L)$ and $\eta = k g \rho_0 z_e / \mu$. The variable r is defined by

$$R = 1 + r, \quad \beta = \beta_0 \, R, \quad R = \exp[C_L(p - p_0)], \tag{4}$$

and represents the deviation of R from the value of 1 (which corresponds to the reference pressure p_0). Eq. 3 is linear for incompressible formations and when gravity is not considered ($\eta' = 0$), and very weakly non-linear otherwise. Because of its generality and robustness, Eq. 3 is the fundamental equation of flow used in the TD analysis. If the necesary conditions are met, TD solutions based on Eq. 2 can be easily obtained following the same approach.

There are two stages in the TD method, the Decomposition stage and the Reconstitution stage. In the Decomposition stage the original PDE is decomposed by using successive levels of integral transforms. The first step in this stage involves the application of the Laplace transform to eliminate the time dependency of the original PDE. The resulting equation is then subjected to successive finite integral (for space) transforms. Since virtually all boundaries in petroleum reservoirs are "no-flow" (i.e. Dirichlet-type), the finite cosine transform is employed. Each level of finite cosine transform eliminates one active dimension, until single point equations remain. The original PDE is thus decomposed into much simpler point algebraic equations, for which solutions are obtained in the transformed space. In the Reconstitution stage, solutions in space and time are obtained by applying succesive levels of inverse transforms. The development of the TD method is described in detail in the following sections.

Step 1: The Laplace Transform of the PDE. The Laplace transform of Eq. 3 yields

$$\begin{aligned} \Lambda(\Psi) &= \nabla \cdot \left[\lambda \nabla \Psi - \eta \left(C_\beta \Psi + 1/s\right)\right] \\ &= C_T \left[s\Psi - r(0)\right] + \ddot{q}, \end{aligned} \tag{5}$$

where $\Lambda()$ is the operator defined in Eq. 5, s is the Laplace domain parameter, $r(0)$ is the distribution of r at $t = 0$,

$$C_\beta = 2 + \bar{r}\,, \tag{6}$$

and

$$\Psi = \Psi(s) = \mathcal{L}\{r\}, \qquad \ddot{q} = \ddot{q}(s) = \mathcal{L}\{q\}, \tag{7}$$

with $\mathcal{L}\{\}$ denoting the Laplace transform of the quantity in braces. Any time-variable $q(t)$ which has a Laplace transform can be considered. The term C_β is obtained from the linearization of

$$2r + r^2 = (2 + r) \; r \simeq C_\beta \, r$$

over the interval from $t = 0$ to $t = t$, and

$$\bar{r} = (1/t) \int_0^t r \; dt = (1/t) \mathcal{L}^{-1}\{\Psi/s\}\,.$$

For small pressure differentials the approximation $C_\beta \simeq 2$ can be used with negligible effects on accuracy.

The TD Method in One Dimension

The boundary conditions in the one-dimensional problem depicted in Fig. 1 are

$$\begin{aligned} r'(x = 0) = r'(x_1 = 0) = u_0 = 0, \\ r'(x = X_{max}) = r'(x_3 = X_3) = u_3 = 0 \end{aligned} \tag{8}$$

indicating no-flow at the outermost boundaries, and

$$r_i'(x_1 = X_1) = u_1(t), \quad r_i'(x_2 = X_2) = u_2(t), \tag{9}$$

which describe internal boundaries which are unknown functions of time. The subscripted x_i ($i \equiv 1,2,3$) denote local coordinates, while the global coordinates have no subscripts. The same convention will be used in the remainder of this paper.

Neglecting gravity, in the i-th ($i = 1,2,3$) locally homogeneous subdomains the governing Laplace-transformed equation of flow is

$$\Lambda \cdot \Psi_i = \lambda_i \frac{d^2\Psi_i}{dx_i{}^2} - C_T\, s\, \Psi_i = -C_T\, r_i(0) + \ddot{q}_i, \quad (10)$$

with boundary conditions

$$\Psi_1'(x_1 = 0) = U_0 = 0,\ \Psi_3'(x_3 = X_3) = U_3 = 0, \quad (11)$$

and

$$\begin{aligned} &\Psi_1'(x_1 = X_1) = U_1, \quad \Psi_2'(x_2 = 0) = \epsilon_1 U_1, \\ &\Psi_2'(x_2 = X_2) = U_2, \quad \Psi_3'(x_3 = 0) = \epsilon_2 U_2, \end{aligned} \quad (12)$$

where $\Psi_i' = \mathcal{L}\{r_i' = \frac{dr_i}{dx_i}\}$, $U_k = \mathcal{L}\{u_k(t)\}$ ($k = 0,\ldots,3$), and $\epsilon_i = k_i/k_{i+1}$. These boundary conditions incorporate the tangent law at the boundary (continuity of fluxes).

Step 2: The Finite Integral Transform. For reasons already explained, the Finite Cosine Transform[4] (FCT) is selected. Taking the FCT of Eq. 10 yields

$$\begin{aligned} \lambda_i\, [-\frac{n^2\pi^2}{X_i^2}\, \Theta_i + (-1)^n\, \Psi_{iX}' - \Psi_{i0}'] \\ - C_T\, s\, \Theta_i = -C_T\, \hat{r}_i(0) + \hat{q}_i, \end{aligned} \quad (13)$$

where

$$\Theta_i(s,n) = \mathcal{F}_C\{\Psi_i\} = \int_0^{X_i} \Psi_i \cos\left(\frac{n\pi x_i}{X_i}\right) dx_i, \quad (14)$$

$\hat{r}_i(0) = \mathcal{F}_C\{r_i(0)\}$, $\hat{q}_i = \hat{q}_i(s,n) = \mathcal{F}_C\{\ddot{q}_i\}$, $\Psi_{i0}' = \Psi_i'(x_i = 0)$, $\Psi_{iX}' = \Psi_i'(x_i = X_i)$, and $\mathcal{F}_C\{\}$ denotes the FCT of the quantity in the brackets. It should be pointed out that $r_i(0)$ need not be a constant; any known function of x_i for which a FCT exists is acceptable. As for the source/sink term $\hat{q}_i$, if $\tilde{q} \neq 0$ for $X_{ib} \leq x_i \leq X_{ie}$ (see **Fig. 1**), then the properties of the FCT yield

$$\hat{q}_i = \begin{cases} \dfrac{\ddot{q}X_i}{n\pi}\left[\sin\left(\dfrac{n\pi X_{ie}}{X_i}\right) - \sin\left(\dfrac{n\pi X_{ib}}{X_i}\right)\right] & n > 0, \\ \ddot{q}(X_{ie} - X_{ib}) & n = 0. \end{cases} \quad (15)$$

The flexibility which Eq. 15 affords is obvious, as it allows the positioning of wells anywhere in the subdomains. Eq. 13 then yields

$$\Theta_i = a_i\, \Psi_{i,B0}' + b_i\, \Psi_{i,BX}' + c_i, \quad (16)$$

where

$$a_i(s,n) = \frac{-\tau_i^2}{n^2 + \omega_i^2}, \quad b_i(s,n) = (-1)^{n+1} a_i, \quad (17)$$

$$c_i = c_i(s,n) = \frac{\omega_i^2}{n^2 + \omega_i^2}\, \frac{\hat{r}_i(0)}{s} - \frac{\hat{q}_i}{\lambda_i}\, \frac{\tau_i^2}{n^2 + \omega_i^2}, \quad (18)$$

and

$$\tau_i = \frac{X_i}{\pi}, \quad \omega_i = \tau_i\, \sigma_i\,, \quad \sigma_i = \sqrt{\frac{C_T\, s}{\lambda_i}}. \quad (19)$$

Eq. 16 is a simple, single-point algebraic equation, and represents the decomposed form of the original one-dimensional PDE. If both $\Psi_{i,B0}'$ and $\Psi_{i,BX}'$ are known (as in the case of a homogeneous system), the decomposition stage ends here.

Step 3: The Internal Boundary Conditions. In heterogeneous systems with multiple subdomains, the internal boundary conditions must be determined next. The pressures being equal on both sides of the boundary between subdomains 1 and 2 in **Fig. 1**, $\Psi_1(x_1 = X_1) = \Psi_2(x_2 = 0)$. Applying the inverse FCT on the governing equations in the two subdomains,

$$\begin{aligned} &\frac{1}{X_1}\Theta_1(s,0) + \frac{2}{X_1}\sum_{n=1}^{\infty}\Theta_1(s,n)\cos\left(\frac{n\pi X_1}{X_i}\right) \\ &= \frac{1}{X_2}\Theta_2(s,0) + \frac{2}{X_2}\sum_{n=1}^{\infty}\Theta_2(s,n)\cos\left(\frac{n\pi 0}{X_2}\right), \end{aligned} \quad (20)$$

from which we obtain the equation

$$F_1\, U_0 + G_1\, U_1 + H_1\, U_2 = R_1, \quad (21)$$

where

$$F_1(s) = \frac{1}{X_1}\left[a_1(s,0) + 2\sum_{n=1}^{\infty}(-1)^n a_1(s,n)\right], \quad (22)$$

$$\begin{aligned} G_1(s) = &\frac{1}{X_1}\left[b_1(s,0) + 2\sum_{n=1}^{\infty}(-1)^n b_1(s,n)\right] \\ &- \frac{\epsilon_1}{X_2}\left[a_2(s,0) + 2\sum_{n=1}^{\infty} a_2(s,n)\right], \end{aligned} \quad (23)$$

$$H_1(s) = -\frac{1}{X_2}\left[b_2(s,0) + 2\sum_{n=1}^{\infty} b_2(s,n)\right], \quad (24)$$

and

$$\begin{aligned} R_1(s) = &\frac{1}{X_2}\left[c_2(s,0) + 2\sum_{n=1}^{\infty} c_2(s,n)\right] \\ &- \frac{1}{X_1}\left[c_1(s,0) + 2\sum_{n=1}^{\infty}(-1)^n c_1(s,n)\right]. \end{aligned} \quad (25)$$

The analytically available limits[5] of the series in Eqs. 22 through 25 result in the closed forms

$$F_1 = -\frac{1}{\sigma_1 \sinh(\pi\omega_1)}, \tag{26}$$

$$G_1 = \frac{1}{\sigma_1 \tanh(\pi\omega_1)} + \frac{\epsilon_1}{\sigma_2 \tanh(\pi\omega_2)}, \tag{27}$$

$$H_1 = -\frac{1}{\sigma_2 \sinh(\pi\omega_2)}, \tag{28}$$

which are trivial to compute. If $r_i(0) = r_{ic}$ (i.e. a constant), the closed form for R_1 is

$$\begin{aligned} R_1 =& \frac{r_{2c} - r_{1c}}{s} \\ &- \frac{\ddot{q}_2}{\lambda_2}\frac{1}{\sigma_2^2}\left[\frac{\sinh(\omega_2\pi - \sigma_2 X_{2b}) - \sinh(\omega_2\pi - \sigma_2 X_{2e})}{\sinh(\omega_2\pi)}\right] \\ &+ \frac{\ddot{q}_1}{\lambda_1}\frac{1}{\sigma_1^2}\left[\frac{\sinh(\sigma_1 X_{1e}) - \sinh(\sigma_1 X_{1b})}{\sinh(\omega_1\pi)}\right]. \end{aligned} \tag{29}$$

In an entirely analogous manner, the equation

$$F_2\, U_1 + G_1\, U_2 + H_2\, U_3 = R_2, \tag{30}$$

is obtained from subdomains 2 and 3. For any subdomain i other than the first the nominator of F_i in Eq. 26 must be changed to ϵ_{i-1}. Eqs. 21 and 30 are the equations which describe the unknown internal boundary conditions. Since $U_0 = U_3 = 0$, the unknown $U_1 = U_1(s)$ and $U_2 = U_2(s)$ are readily obtained from the two equations. In general, if there are N subdomains with locally homogeneous properties, these define $N+1$ boundaries of which 2 (the outermost) are known and the remaining $N_B = N-1$ are the internal unknown boundaries. Writing the resulting $N_{EQ} = N_B$ simultaneous equations in a matrix notation, we have

$$\mathbf{M}\,\vec{U} = \vec{R}\,, \tag{31}$$

where $\mathbf{M}$ is the coefficient matrix, $\vec{R}$ is the 'known' right-hand side vector, and $\vec{U}$ is the vector of the Laplace transform of the unknown Dirichlet conditions Ψ' at the internal boundaries. Solution of Eq. 31 requires values for the Laplace domain parameter s. For a desired observation time t, the Stehfest algorithm[6,7] provides the s as

$$s_\nu = \frac{\ln 2}{t}\nu\,, \quad \nu = 1, \ldots, N_S\,, \tag{32}$$

where N_S is the number of summation terms in the algorithm, and N_S is an even number. Optimum values for N_S were discussed extensively by Moridis *el al.*[3]. Solution of Eq. 31 yields the set of N_S vectors

$$\vec{U}_\nu = \mathbf{M}_\nu^{-1}\,\vec{R}_\nu\,, \quad \nu = 1, \ldots, N_S\,. \tag{33}$$

Steps 1 through 3 represent the Decomposition stage. The Reconstitution stage is described in Steps 4 and 5.

Step 4: The Laplace Domain Solution. Once the $\vec{U}_\nu$ becomes known, then the Laplace transform Ψ_ν of r and at any point x_ℓ within a subdomain i with boundaries U_ξ and $U_{\xi+1}$ is given by the inverse FCT as

$$\Psi_i(s_\nu, x_\ell) = a_{iT}\, U_\xi(\nu) + b_{iT}\, U_{\xi+1}(\nu) + c_{iT}, \tag{34}$$

where

$$\begin{aligned} a_{iT} =& \frac{1}{X_i}\left[a_i(s_\nu, 0) + 2\sum_{n=1}^{\infty} a_i(s_\nu, n)\cos\left(\frac{n\pi x_\ell}{X_i}\right)\right] \\ =& \frac{\epsilon_{i-1}\cosh(\omega_i\pi - \sigma_i x_\ell)}{-\sigma_i \sinh(\pi\omega_i)} \\ =& \epsilon_{i-1}\, F_1 \cosh(\omega_i\pi - \sigma_i x_\ell), \end{aligned} \tag{35}$$

$$\begin{aligned} b_{iT} =& \frac{1}{X_i}\left[b_i(s_\nu, 0) + 2\sum_{n=1}^{\infty} b_i(s_\nu, n)\cos\left(\frac{n\pi x_\ell}{X_i}\right)\right] \\ =& \frac{\cosh(\sigma_i x_\ell)}{\sigma_i \sinh(\pi\omega_i)} = -F_1 \cosh(\sigma_i x_\ell)\,, \end{aligned} \tag{36}$$

and are trivial to compute. Similarly, the closed form of c_{iT} is

$$\begin{aligned} c_{iT} =& \frac{1}{X_i}\left[c_i(s_\nu, 0) + 2\sum_{n=1}^{\infty} c_i(s_\nu, n)\cos\left(\frac{n\pi x_\ell}{X_i}\right)\right] \\ =& \frac{\ddot{q}_i}{2\lambda_i}\frac{1}{\sigma_i^2}\left\{\frac{\sinh[\omega_i\pi - \sigma_i(X_{ie} + x_\ell)]}{\sinh(\omega_i\pi)}\right. \\ &+ \frac{\sinh[\omega_i\pi - \sigma_i(X_{ie} - x_\ell)]}{\sinh(\omega_i\pi)} \\ &- \frac{\sinh[\omega_i\pi - \sigma_i(X_{ib} + x_\ell)]}{\sinh(\omega_i\pi)} \\ &\left.- \frac{\sinh[\omega_i\pi - \sigma_i(X_{ib} - x_\ell)]}{\sinh(\omega_i\pi)}\right\} + \frac{r_{ic}}{s}. \end{aligned} \tag{37}$$

Step 5: The Solution at Time t. To obtain a solution at a time t at a number of desired points x_ℓ, all vectors $\vec{\Psi}_\nu$, $\nu = 1, \ldots, N_S$ are needed. The unknown vector $\vec{r}$ at time t is obtained by using the Stehfest algorithm[6,7] to numerically invert the Laplace solutions $\vec{\Psi}_\nu$. The procedure is described by the following equations:

$$\vec{r}(t) = \frac{\ln 2}{t}\sum_{\nu=1}^{N_S} W_\nu \cdot \vec{\Psi}_\nu\,, \tag{38}$$

and

$$W_\nu = V_\nu \sum_{\kappa=L_0}^{L_M} \frac{\kappa^{\frac{N_S}{2}}(2\kappa)!}{(\frac{N_S}{2}-\kappa)!\kappa!(\kappa-1)!(\nu-\kappa)!(2\kappa-\nu)!}, \tag{39}$$

where $V_\nu = (-1)^{\frac{N_S}{2}+\nu}$, $L_0 = \frac{1}{2}(\nu+1)$, and $L_M = \min\{\nu, \frac{N_S}{2}\}$. $\vec{R}$ is then computed as

$$\vec{R}(t) = \vec{I} + \vec{r}(t), \tag{40}$$

where $\vec{I}$ is the unit vector. The pressure vector $\vec{p}$ can be obtained from Eq. 3 as $p = p_0 + C_L^{-1} \ln R$. It must be noted that because of its formulation, the TD method provides semi-analytical solutions which are fully differentiable and integral; continuous velocity fields are thus easily determined, and mass balance calculations over the subdomains become trivial.

The TD Method in Two Dimensions

For the two-dimensional domain in Fig. 2 the boundary conditions are

$$\begin{aligned} r'(x_1=0,y_1) &= u_1^\star = r'(x_3=X_3,y_3) = u_2^\star = 0 \\ r'(x_4=0,y_1) &= u_3^\star = r'(x_7=X_7,y_7) = u_4^\star = 0 \\ r'(x_1,y_1=0) &= u_5^\star = r'(x_4,y_4=Y_4) = u_6^\star = 0 \\ r'(x_2,y_2=0) &= u_7^\star = r'(x_5,y_5=Y_5) = u_8^\star = 0 \\ r'(x_3,y_3=0) &= u_9^\star = r'(x_5,y_5=Y_5) = u_{10}^\star = 0, \end{aligned} \tag{41}$$

indicating no-flow across the reservoir perimeter, and

$$\begin{aligned} r'(x_i=X_i,y_i) &= u_i(t,y_i), \quad i=1,2 \\ r'(x_i=X_i,y_i) &= u_{i-1}(t,y_i), \quad i=4,5 \\ r'(x_i=x_i,Y_i) &= u_{i+4}(t,x_i), \quad i=1,2,3 \end{aligned} \tag{42}$$

describing unknown internal boundaries. Eq. 42 represents the prevailing conditions as $lim_{\delta\to 0}\Psi'(x=X_i-\delta)$ or $\Psi'(y_i=Y_i-\delta)$. The boundary conditions at $\Psi'(x_{i+1}=\delta)$ and $\Psi'(y_{i+1}=\delta)$ are easily obtained by applying the tangent law as $\epsilon_{ix}\Psi'(X_i+\delta)$ and $\epsilon_{iy}\Psi'(X_i+\delta)$ respectively.

Neglecting gravity, in the locally homogeneous subdomain 1 the Laplace-transformed equation of flow is

$$\begin{aligned} \Lambda(\Psi_1) &= \lambda_{1x}\frac{\partial^2\Psi_1}{\partial x_1{}^2} + \lambda_{1y}\frac{\partial^2\Psi_1}{\partial y_1{}^2} - C_T\, s\, \Psi_1 \\ &= -C_T\, r_i(0) + \ddot{q}_1, \end{aligned} \tag{43}$$

with boundary conditions

$$\Psi_1'(x_1=0,y_1) = U_0^\star = \Psi_3'(x_1,y_1=0) = U_5^\star = 0, \tag{44}$$

and

$$\begin{aligned} \Psi_1'(x_1=X_1,y_1) &= \Psi_2'(x_2=0,y_2) = U_1, \\ \Psi_1'(x_1,y_1=Y_1) &= \Psi_4'(x_4,y_4=0) = U_3, \end{aligned} \tag{45}$$

where $\Psi_i' = \mathcal{L}\{r_i'\}$, and $U_k = \mathcal{L}\{u_k\}$ $(k=1,3)$.

Step 2: The Finite Integral Transforms. Taking the FCT of Eq. 43 with respect to y yields

$$\begin{aligned} \lambda_{1x}\frac{d^2\Theta_1}{dx_1{}^2} + \lambda_{1y}\left[-\frac{n^2\pi^2}{Y_1^2}\,\Theta_1 - U_5^\star + (-1)^n U_5(x_1)\right] \\ - C_T\, s\, \Theta_1 = -C_T\, \hat{r}_i(0) + \hat{q}_1, \end{aligned} \tag{46}$$

where

$$\Theta_1 = \mathcal{F}_C\{\Psi_1\} = \int_0^{Y_1} \Psi_1 \cos\left(\frac{n\pi y_1}{Y_1}\right) dy_1, \tag{47}$$

and $\Theta_1 = \Theta_1(s,x_1,n)$. Eq. 46 incorporates the boundary conditions at $y_1=0$ and $y_1=Y_1$. The term $\hat{r}_1(0) = \mathcal{F}_C\{r_1(0)\}$ is now a function of x, and $\hat{q}_1 = \hat{q}_1(s,x,n) = \mathcal{F}_C\{\ddot{q}_1\}$ is obtained from Eq. 15 with y substituted for x. The boundary conditions then become

$$\hat{U}_1^\star = \mathcal{F}_C\{U_1^\star\} = 0, \quad \hat{U}_1 = \hat{U}_1(n) = \mathcal{F}_C\{U_1(y_1)\}. \tag{48}$$

Taking the FCT of Eq. 46 with respect to x yields

$$\begin{aligned} &\lambda_{1x}\left[-\frac{m^2\pi^2}{X_1^2}\,\Phi_1 - \hat{U}_1^\star + (-1)^m\hat{U}_1(n)\right] \\ &+\lambda_{1y}\left[-\frac{n^2\pi^2}{Y_1^2}\,\Phi_1 - \hat{U}_5^\star + (-1)^m\hat{U}_5(m)\right] \\ &-C_T\, s\, \Phi_1 = -C_T\, \hat{\hat{r}}_1(0) + \hat{\hat{q}}_1, \end{aligned} \tag{49}$$

where $\Phi_1 = \Phi_1(s,m,n)$,

$$\Phi_1 = \mathcal{F}_C\{\Theta_1\} = \int_0^{X_1} \Theta_1 \cos\left(\frac{n\pi x_1}{X_1}\right) dx_1, \tag{50}$$

and

$$\hat{\hat{r}}_1(0) = \mathcal{F}_C\{\hat{r}_1(0)\}, \ \hat{\hat{q}}_1 = \hat{\hat{q}}_1(s,n,m) = \mathcal{F}_C\{\hat{q}_1\}. \tag{51}$$

From Eq. 49 we derive

$$\begin{aligned} \Phi_1 = h_{1W}\,\hat{U}_1^\star + h_{1E}\,\hat{U}_1(n) \\ + h_{1S}\,\hat{U}_5^\star + h_{1N}\,\hat{U}_5(m) + h_{1C}, \end{aligned} \tag{52}$$

where

$$\begin{aligned} h_{1W}(s,m,n) &= \frac{-\lambda_{1x}\,\tau_{1x}^2}{m^2+\tau_{1x}^2}, \ h_{1E} = (-1)^{m+1}h_{1W}, \\ h_{1S}(s,m,n) &= \frac{-\lambda_{1y}\,\tau_{1x}^2}{m^2+\tau_{1x}^2}, \ h_{1N} = (-1)^{n+1}h_{1S}, \end{aligned} \tag{53}$$

$$h_{1C} = h_{1C}(s,m,n) = \frac{[C_T\ \hat{\hat{r}}_1(0) - \hat{\hat{q}}_1]}{\lambda_{1x}} \frac{\tau_{1x}^2}{m^2 + \tau_{1x}^2}, \quad (54)$$

and

$$\tau_{1x} = \frac{X_1}{\pi} = \frac{\omega_{1x}}{\sigma_{1x}}\ ,\ \sigma_{1x} = \sqrt{n^2 \frac{\lambda_{1y}}{\lambda_{1x}} \frac{\pi^2}{Y_1^2} + \frac{C_T\ s}{\lambda_{1x}}}. \quad (55)$$

Eq. 52 is a simple, single-point algebraic equation, and represents the decomposed form of the original PDE. The same form will be obtained regardless of the path of integral transforms, i.e. of whether the order of the FCT is (y,x) or (x,y). This property will be used in the next subsection. If all the boundary conditions are known (as in the case of a single domain), the decomposition stage ends here.

Step 3: The Internal Boundary Conditions. The pressures being equal on both sides of the boundary at $x_1 = X_1, x_2 = 0$ (**Fig. 2**), $\Theta_1(x_1 = X_1) = \Theta_2(x_2 = 0)$. Applying the inverse FCT with respect to $m \rightarrow x$ in the equations in the two subdomains,

$$\begin{aligned} &\frac{1}{X_1}\Phi_1(s,0,n) + \frac{2}{X_1}\sum_{m=1}^{\infty}(-1)^n\ \Phi_1(s,m,n) \\ &= \frac{1}{X_2}\Phi_2(s,0,n) + \frac{2}{X_2}\sum_{m=1}^{N_T}\Phi_2(s,m,n), \end{aligned} \quad (56)$$

and the equation of the first internal boundary is

$$\begin{aligned} &A_{1L}\ \hat{U}_1^* + A_{1C}\ \hat{U}_1(n) + A_{1R}\ \hat{U}_2(n) \\ &+ \sum_{m=0}^{\infty}[A_{1UL}\ \hat{U}_5(m) + A_{1UR}\ \hat{U}_6(m) \\ &\qquad A_{1DL}\ \hat{U}_5^* + A_{1DR}\ \hat{U}_6^*] = S_1, \end{aligned} \quad (57)$$

where the analysis described in the one-dimensional problem yields

$$A_{1L}(s,n) = -\frac{1}{\sigma_{1x}\ \sinh(\pi\omega_{1x})}, \quad (58)$$

$$A_{1C}(s,n) = \frac{1}{\sigma_{1x}\ \tanh(\pi\omega_{1x})} + \frac{\epsilon_{1x}}{\sigma_{2x}\ \tanh(\pi\omega_{1x})}, \quad (59)$$

$$A_{1R}(s,n) = -\frac{1}{\sigma_{2x}\ \sinh(\pi\omega_{2x})} \quad (60)$$

$$\begin{aligned} S_1(s,n) &= C_T\left(\frac{r_{2c}}{\lambda_{2x}\sigma_{2x}} - \frac{r_{1c}}{\lambda_{1x}\sigma_{1x}}\right) \\ &- \frac{\ddot{q}_2}{\lambda_{2x}\sigma_{2x}^2}\left[\frac{\sinh(\omega_{2x}\pi - \sigma_{2x}X_{2b})}{\sinh(\omega_{2x}\pi)}\right. \\ &\qquad \left. - \frac{\sinh(\omega_{2x}\pi - \sigma_{2x}X_{2e})}{\sinh(\omega_{2x}\pi)}\right] \\ &+ \frac{\ddot{q}_1}{\lambda_{1x}\sigma_{1x}^2}\left[\frac{\sinh(\sigma_{1x}X_{1e}) - \sinh(\sigma_{1x}X_{1b})}{\sinh(\omega_{1x}\pi)}\right], \end{aligned} \quad (61)$$

$$A_{1UL} = \begin{cases} \dfrac{h_{1N}(s,0,n)}{X_1} & \text{for } m = 0 \\ \dfrac{2(-1)^m h_{1N}(s,m,n)}{X_1} & \text{for } m > 0, \end{cases} \quad (62)$$

$$A_{1UR} = \begin{cases} -\dfrac{h_{2N}(s,0,n)}{X_2} & \text{for } m = 0 \\ -\dfrac{2h_{2N}(s,m,n)}{X_2} & \text{for } m > 0, \end{cases} \quad (63)$$

$$A_{1DL} = \begin{cases} \dfrac{h_{1S}(s,0,n)}{X_1} & \text{for } m = 0 \\ \dfrac{2(-1)^m h_{1S}(s,m,n)}{X_1} & \text{for } m > 0, \end{cases} \quad (64)$$

and

$$A_{1DR} = \begin{cases} -\dfrac{h_{2S}(s,0,n)}{X_2} & \text{for } m = 0 \\ -\dfrac{2h_{2S}(s,m,n)}{X_2} & \text{for } m > 0. \end{cases} \quad (65)$$

The terms A_{1UL}, A_{1UR}, A_{1DL}, and A_{1DR} are functions of (s,m,n). The term N_T in Eq. 57 indicates the number of terms in the truncated series. We have three additional equations at the interfaces $x_2 = X_2, x_3 = 0$ (boundary number 2), $x_4 = X_4, x_5 = 0$ (boundary 3), and $x_5 = X_5, x_6 = 0$ (boundary 4), obtained from Eq. 57 by substituting the appropriate boundary number for the subscript 1. The equations total $4(N_T + 1)$, and are valid for all n.

The equality of pressures at the $y_1 = Y_1, y_4 = 0$ boundary (**Fig. 2**) between subdomains 1 and 4 dictates that $\Theta_1(y_1 = Y_1) = \Theta_4(y_4 = 0)$. We follow the same procedure described in the development of the boundary equations along the axis of x. However, in this case we apply the inverse FCT transform to the Eq. 52 derived from the FCT transformation through the path (x,y), as opposed to the path (y,x) used previously. Following the same analysis described above, we obtain the equation at the 5th internal boundary (described by $\hat{U}_5$) as

$$\begin{aligned} &B_{5D}\ \hat{U}_5^* + B_{5C}\ \hat{U}_5(m) + B_{5U}\ \hat{U}_8^* \\ &+ \sum_{n=0}^{N_T}[B_{5DR}\ \hat{U}_1(n) + B_{5UR}\ \hat{U}_3(n) \\ &\qquad B_{5DL}\ \hat{U}_1^* + B_{5UL}\ \hat{U}_3^*] = S_5, \end{aligned} \quad (66)$$

where

$$B_{5D}(s,m) = -\frac{1}{\sigma_{1y}\ \sinh(\pi\omega_{1y})}, \quad (67)$$

$$B_{5C}(s,m) = \frac{1}{\sigma_{1y}\ \tanh(\pi\omega_{1y})} + \frac{\epsilon_{4y}}{\sigma_{4y}\ \tanh(\pi\omega_{4y})} \quad (68)$$

$$B_{5U}(s,m) = -\frac{1}{\sigma_{4y}\sinh(\pi\omega_{4y})}, \tag{69}$$

$$\begin{aligned} S_5(s,n,m) = {} & C_T\left(\frac{r_{4c}}{\lambda_{4y}\sigma_{4y}} - \frac{r_{1c}}{\lambda_{1y}\sigma_{1y}}\right) \\ & -\frac{\ddot{q}_2}{\lambda_{4y}\sigma_{4y}^2}\left[\frac{\sinh(\omega_{4y}\pi - \sigma_{4y}Y_{4b})}{\sinh(\omega_{4y}\pi)}\right. \\ & \left. - \frac{\sinh(\omega_{4y}\pi - \sigma_{4y}Y_{4e})}{\sinh(\omega_{4y}\pi)}\right] \\ & +\frac{\ddot{q}_1}{\lambda_{1y}\sigma_{1y}^2}\left[\frac{\sinh(\sigma_{1y}Y_{1e}) - \sinh(\sigma_{1y}Y_{1b})}{\sinh(\omega_{1y}\pi)}\right], \end{aligned} \tag{70}$$

$$B_{5UL} = \begin{cases} -\dfrac{h_{4W}(s,m,0)}{Y_4} & \text{for } n = 0 \\ -\dfrac{2h_{4W}(s,m,n)}{Y_4} & \text{for } n > 0, \end{cases} \tag{71}$$

$$B_{5UR} = \begin{cases} -\dfrac{h_{4E}(s,m,0)}{Y_4} & \text{for } n = 0 \\ -\dfrac{2h_{4E}(s,m,n)}{Y_4} & \text{for } n > 0, \end{cases} \tag{72}$$

$$B_{5DL} = \begin{cases} \dfrac{h_{1W}(s,m,0)}{Y_1} & \text{for } n = 0 \\ \dfrac{2(-1)^n h_{1W}(s,m,n)}{Y_1} & \text{for } n > 0, \end{cases} \tag{73}$$

and

$$B_{5DR} = \begin{cases} \dfrac{h_{1E}(s,m,0)}{Y_1} & \text{for } n = 0 \\ \dfrac{2^n h_{1E}(s,m,n)}{Y_1} & \text{for } n > 0. \end{cases} \tag{74}$$

The terms B_{5UL}, B_{5UR}, B_{5DL}, and B_{5DR} are functions of (s,m,n). The terms ω_{iy}, τ_{iy}, and σ_{iy} are obtained from Eq. 55 by cyclic substitution. With the two additional equations are obtained at the interfaces $y_2 = Y_2, y_5 = 0$ (boundary number 6) and $y_3 = Y_3, y_6 = 0$ (boundary 7), $3(N_T + 1)$ simultaneous equations are added (valid for all m). The total number of unknowns and equations is $N_{EQ} = N_B(N_T + 1)$ ($N_B = 7$ the number of unknown boundaries). Of special interest is the case of subdomains connected along a single direction (e.g. when the domain is composed of subdomains 1, 2, and 3). The terms in the summations of Eqs. 57 and 66 are then all known quantities, and the size of the matrix is sharply reduced from order $N_{EQ} = N_B(N_T + 1)$ to order $N_{EQ} = N_B$. The resulting matrix M in Eq. 31 in a sparse matrix which is ideally suited to LU decomposition.

If the convergence of $\sum_{m=0}^{\infty} A_{1UL}\hat{U}_5(m)$ in Eq. 57 (and other such sums) is not satisfactory, an alternative method may be used to avoid inordinately enlarging the order of the matrices by increasing N_T. Then the unknown $\Psi' = \Psi'(x)$ is assumed to be described by

$$\Psi'(x) = v_0 + v_1\, x + v_2 \exp(v_3 x) + v_4\, x \exp(v_5 x), \tag{75}$$

which has an easily determined FCT. In our experience, this form has performed exceptionally well. The quantity $x \exp(v_5 x)$ in Eq. 75 is particularly well suited to the description of wells in the subdomains. This approach reduces the order of the matrix from $N_{EQ} = N_B(N_T + 1)$ to $N_{EQ} = 7\ N_B$. An important point is that TD does not require regural grid systems; irregular geometries (such as the one in **Fig. 3**) pose no partricular problems.

Step 4: The Laplace Domain Solution. In the first step of the Reconstitution stage, application of two successive inverse FCT yields Ψ at any point (x_ℓ, y_ℓ) within a subdomain i as

$$\begin{aligned} \Psi_i(s_\nu, x_\ell, y_\ell) = {} & \frac{1}{X_i Y_i}\Bigg[\Phi_i(s_\nu,0,0) + \\ & 2\sum_{m=1}^{M_T}\Phi_i(s_\nu,m,0)\cos\left(\frac{m\pi x_\ell}{X_i}\right) + \\ & 2\sum_{n=1}^{N_T}\Phi_i(s_\nu,0,n)\cos\left(\frac{n\pi y_\ell}{Y_i}\right) + \\ & 4\sum_{n=1}^{N_T}\sum_{m=1}^{M_T}\Phi_i(s_\nu,m,n)\cos\left(\frac{m\pi x_\ell}{X_i}\right)\cos\left(\frac{n\pi y_\ell}{Y_i}\right)\Bigg], \end{aligned} \tag{76}$$

and is readily computed by simple substitution with Φ_i obtained from Eq. 52. The $\sum_k \Phi\cos(kx)$ can be written as $\sum_k \Phi\, z_1^k - \sum_k \Phi z_2^k$, where $z_1 = \exp(j\pi)$, $z_1 = \exp(-j\pi)$, and $j = \sqrt{-1}$. The epsilon algorithm of McDonald[8] (valid for this type of power series) can then be used to significantly accelerate the convergence of the series in Eq. 76.

Step 5: The Solution at Time t. The solution at a time t is obtained by following the same procedure described in detail in the one-dimensional problem.

The TD method eliminates the stability and accuracy problems caused by the treatment of the space and time derivatives in standard FD simulators. Because of the Laplace transform formulation, an unlimited timestep size is possible. In a standard FD method, there are three sources of error: the time-related truncation error, the space-related truncation error, and the roundoff error. Because the time domain is not discretized, there is no time-related truncation error in the TD method. The use of finite integral transforms requires only a very coarse grid which does not introduce any space-related truncation error. The sources of error in the TD method are the error attributed to the numerical inversion of the Laplace solution, the error introduced by the inverse FCT's, and the roundoff error.

The numerical inversion of the Laplace transforms creates very little (if any) error[3], which for smooth time functions can be at the level of machine accuracy. The inversion of the FCT's introduces an error (stemming mainly from the truncation of the corresponding infinite series) which can be extremely small, and is reduced by increasing N_T. The ability to use an unlimited timestep size bounds the accumulation of roundoff error by an upper limit defined as the roundoff error accumulated after the N_S solutions of the N_{EQ} equations. Thus, the TD solution is inherently more accurate than the standard FD method. It offers a stable, non-increasing roundoff error irrespective of the time of observation t_{obs}, because calculations have to be performed at this time only using a $\Delta t = t_{obs}$; on the other hand, calculations in a standard FD method have to be performed at all the intermediate times of the discretized time domain, continuously accumulating roundoff error in the process.

Compared to a standard FD model, the TD method reduces the computer memory requirements, because discretization in time is not needed, and a very coarse grid suffices for the space discretization. Execution times may be significantly reduced because the inverted matrices in the TD method are usually small, and solutions are obtained at the desired points in space and time only, while in standard numerical methods solutions are necessary at all of the points of the discretized time and space domains.

The TD Method in Three Dimensions

Extension of the TD method to three dimensions follows the same procedure. The problem is decomposed from a three-dimensional PDE to a single-point algebraic equation by applying (a) first a Laplace transform, and (b) successive levels of FCT's. By equating pressures at the boundary planes, the transformed boundary conditions are determined, and are used to calculate Ψ at any point of the domain by applying inverse FCT's. The solution at time t is obtained by inverting Ψ using the Stehfest algorithm.

Gravitational Effects and Internal Iterations

The one-dimensional case will be discussed here. Extension to 2 and 3 dimensions is entirely analogous. If gravity is included, the Laplace-transformed equation of flow is

$$\lambda_i \frac{d^2\Psi_i}{dx_i{}^2} - \eta_i \frac{d\Psi_i}{dx_i} - (C_T\, s + \eta_i'\, C_\beta)\, \Psi_i = \frac{\eta_i'}{s} - C_T\, r_i(0) + \ddot{q}_i, \tag{77}$$

with boundary conditions described by Eqs. 11 and 12. Eq. 77 describes either an inclined or a vertical system (when x is taken in the vertical direction). The FCT of Eq. 77 results in

$$\begin{aligned} &\lambda_i \left[-\frac{n^2\pi^2}{X_i^2}\, \Theta_i + (-1)^n\, \Psi_{iX}' - \Psi_{i0}'\right] \\ &-\eta_i \left[-\frac{n\pi}{X_i}\Omega_i + (-1)^n\, \Psi_{iX} - \Psi_{i0}\right] \\ &-(C_T\, s + \eta_i'\, C_\beta)\, \Theta_i = \frac{\hat{\eta}'_i}{s} - C_T\, \hat{r}_i(0) + \hat{q}_i, \end{aligned} \tag{78}$$

where $\Omega_i = \mathcal{F}_S\{\Psi_i\}$, $\hat{\eta}'_i = \mathcal{F}_C\{\eta_i'\}$, and $\mathcal{F}_S\{\}$ denotes the Finite Sine Transform (FST) of the quantity in the brackets. Collecting and rearranging terms, Eq. 77 becomes

$$\begin{aligned} D_{i\Theta}\, \Theta_i + D_{i\Omega}\, \Omega_i = {} & D_{i1}\, \Psi_{i,B0}' + D_{i2}\, \Psi_{i,BX}' \\ & + D_{i3}\, \Psi_{i,B0} + D_{i4}\, \Psi_{i,BX} + D_{iC}, \end{aligned} \tag{79}$$

where

$$D_{i\Theta} = \lambda_i \frac{n^2\pi^2}{X_i^2} + C_T\, s + \eta_i'\, C_\beta, \tag{80}$$

$$D_{i\Omega} = -\eta_i \frac{n\pi}{X_i}, \quad D_{iC} = -\frac{\hat{\eta}'_i}{s} + C_T\, \hat{r}_i(0) - \hat{q}_i, \tag{81}$$

$$D_{i1} = -\lambda_i, \quad D_{i2} = (-1)^n \lambda_i, \tag{82}$$

and

$$D_{i3} = \eta_i, \quad D_{i4} = (-1)^{n+1}\eta_i. \tag{83}$$

It is obvious that inclusion of gravity introduces (a) Ω in addition to Θ, and (b) the boundary conditions $\Psi_{i,B0}$ and $\Psi_{i,BX}$ in addition to $\Psi_{i,B0}'$ and $\Psi_{i,BX}'$. This necessitates an additional equation, which is provided by the requirement that at the internal boundaries not only are the pressures equal, but the pressure derivatives at the boundaries between adjacent subdomains are related through the continuity of fluxes

$$\begin{aligned} &\lambda_i \frac{d\Psi_i}{dx_i} - \eta_i(C_\beta\, \Psi_i + 1/s) \\ &\quad = \lambda_{i+1} \frac{d\Psi_{i+1}}{dx_{i+1}} - \eta_{i+1}(C_\beta\, \Psi_{i+1} + 1/s). \end{aligned} \tag{84}$$

At the interface $\Psi_i = \Psi_{i+1}$, resulting in

$$\begin{aligned} &\lambda_i \frac{d\Psi_i}{dx_i} + C_\beta(\eta_{i+1} - \eta_i)\, \Psi_i \\ &\quad = \lambda_{i+1} \frac{d\Psi_{i+1}}{dx_{i+1}} + (\eta_i - \eta_{i+1})/s. \end{aligned} \tag{85}$$

Taking the FST of Eq. 77 yields

$$\begin{aligned} E_{i\Theta}\, \Theta_i + E_{i\Omega}\, \Omega_i = {} & E_{i1}\, \Psi_{i,B0}' + E_{i2}\, \Psi_{i,BX}' \\ & + E_{i3}\, \Psi_{i,B0} + E_{i4}\, \Psi_{i,BX} + E_{iC}, \end{aligned} \tag{86}$$

where

$$E_{i\Omega} = \left[\lambda_i \frac{n^2\pi}{X_i^2} + C_T\ s + \eta_i'\ C_\beta\right], \tag{87}$$

$$E_{i\Theta} = -\eta_i \frac{n\pi}{X_i}, \quad E_{iC} = -\frac{\bar{\eta}'_i}{s} + C_T\ \bar{r}_i(0) - \bar{q}_i, \tag{88}$$

$$E_{i1} = 0, \quad E_{i2} = 0, \tag{89}$$

and

$$E_{i3} = \lambda_i \frac{n\pi}{X_i}, \quad E_{i4} = (-1)^{n+1} E_{i3}. \tag{90}$$

The terms marked with an overbar in Eq. indicate the FST of the relevant quantities. The need for the FST arises from the fact that Eq. 85 contains derivatives, which, when applied to FST's, result in cosine formulations. These are well behaved at the boundaries, as opposed to the sine formulations which require a very large number of summation terms for convergence. Elimination of Ω_i from Eq. 79 results in

$$\begin{aligned}\Theta_i = W_{i1}\ \Psi'_{i,B0} + W_{i2}\ \Psi'_{i,BX} \\ + W_{i3}\ \Psi_{i,B0} + W_{i4}\ \Psi_{i,BX} + W_{iC},\end{aligned} \tag{91}$$

where

$$W_{i\chi} = \frac{D_{i\chi} - \dfrac{D_{i\Omega}}{E_{i\Omega}}}{D_{i\Theta} - \dfrac{D_{i\Omega}}{E_{i\Omega}}}, \quad \chi \equiv 1, 2, 3, 4, C. \tag{92}$$

A similar equation is provided by the elimination of Θ_i from Eq. 86.

The first equation of the boundary is obtained by equating the Ψ (provided by Eq. 91) at the boundary. The second equation of the boundary is obtained from the tangent law relationship (Eq. 85), in which the Ψ is provided by Eq. 91 and the Ψ' from the equation obtained from the elimination of Θ_i from Eq. 86 . If there N subdivisions in the domain, there are only 2 known boundary conditions (at the outermost domain boundaries). For no-flow outermost boundaries, the domain has $N-1$ unknown boundary $\frac{d\Psi}{dx}$'s and $N+1$ unknown boundary Ψ's, for a total of $N_{EQ} = 2N$ unknowns. Inclusion of gravitational effects thus doubles the number of simultaneous equations. In the resulting Eq. 31 **M** is of order $N_{EQ} = 2 \times N$, and the solution $\vec{U}$ includes both Ψ and Ψ' at the internal boundaries. Ψ which can be determined at any point x_ℓ in the subdomain i by inverting the FCT of Eq. 91.

Inner Iterations. These are required only when the approximations of C_T[3] and of C_β in Eq. 5 are not acceptably accurate. The TD method addresses the problems posed by these weak nonlinearities through an iteration procedure entirely analogous to the treatment of such nonlinearities in FD. The process involves a limited number of inner iterations (2 to 4), during which the values of C_T and C_β are updated and an improved solution r is obtained until a desired convergence criterion is met.

Verification and Test Problems

The TD method was tested using three test problems. The TD solution for the first and third problems were verified through comparison with available analytical solutions. No analytical solutions exist for the second test problem. In all three cases the results obtained with the TD method (TDM) were tested against results obtained using a standard, commercially available implicit FD simulator[9]. Double precision variables with 16 and 20 significant figures were used in all simulations. A variable timestep Δt was used for all test cases in the FD simulator, given by the recursive formula

$$\Delta t_\ell = \min\{M_L \times \Delta t_{\ell-1}, \Delta t_{max}, \Delta t_{\Delta pmax}\} \tag{93}$$

where M_L is a multiplier, Δt_{max} is the maximum permissible Δt, and $\Delta t_{\Delta pmax}$ is the Δt corresponding to a maximum permissible pressure change Δp_{max}. Table 1 shows the M_L, Δt_0, Δt_{max}, and Δp_{max} used in the test problems, as well as the number of timesteps and matrix solutions (i.e. the number of times the system of simultaneous equations in the FD simulator had to be solved) in the simulations. Because of internal iterations, the number of matrix solutions is significantly larger than the number of timesteps.

Verification and Test Problem 1. Test Problem 1 was a problem of flow to a well located at a vertical fracture of length L (perpendicular to the x axis) and depth h in a rectangular (one-dimensional) reservoir. **Table 2** shows the fluid properties. Reservoir properties and dimensions, and discretization information for the FD and TD simulations appear in **Table 3**. The analytical solution of this problem is given by

$$p_D = \mathcal{L}^{-1}\{\Psi_D\}, \ \Psi_D = H_1 + H_2, \tag{94}$$

where

$$H_1 = \frac{\exp(-x_D\sqrt{s})}{s^{1.5}\,[1 - \exp(-2\ X_D\ \sqrt{s})]}, \tag{95}$$

$$H_2 = \frac{\exp[(x_D - 2\ X_D)\sqrt{s}]}{s^{1.5}\,[1 - \exp(-2\ X_D\ \sqrt{s})]}, \tag{96}$$

and

$$p_D = (p_i - p)\frac{k\sqrt{A}}{q\ \mu}, \ t_D = \frac{k\ t}{A\ \phi\ \mu\ C_L}, \ x_D = \frac{x}{\sqrt{A}}. \tag{97}$$

The term X is the length of the reservoir, and A is the cross section in the direction of flow ($= L \times h$). This solution is

a Laplace space solution, and needs to be inverted to obtain the solution in the dimensionless time t_D.

We investigated two subproblems. In Problem 1a we obtained the TD solution using the equation for a single homogeneous domain (as specified). In problem 1b we tested the performance of the TD concept by subdividing the domain (5000 ft) into two subdomains (300 and4200 ft), and comparing the solution to the one from Problem 1a. The two TD solutions were virtually identical, differing in the 8th or 9th decimal place. This confirmed the validity of the concept. All results in Test Problem 1 correspond to both subproblems and are presented together.

Fig. 4 shows the TD solutions at a number of times. The measure of the accuracy of the TD method is given by **Fig. 5**, which compares the TD results to the analytical solution. The observed deviations are extremely small, and the TD method is shown to be practically insensitive to the size of the time increment (thus allowing an unlimited timestep).

In **Fig. 6** we investigate the performance of the TD method as affected by the number of summation terms $N_S = 8$ in the Stehfest algorithm. The solution with a $N_S = 12$ was used as the reference solution. The results confirm previous observations[3], i.e. the value of N_S seems to have little effect on the accuracy of the method for $8 \geq N_S \geq 20$. The implication of this observation is that the method is very efficient because a limited number of summation terms is needed, thus reducing the computational requirements. Although the TD method seems to be slightly more sensitive to the value of N_S than in the LTFD method[3] (where a $N_S = 8$ was sufficient for most applications), for practical purposes a $N_S = 10$ provides a highly accurate solution; the additional accuracy for $N_S > 12$ is marginal. Unless otherwise specified, a $N_S = 12$ is used in the simulations.

Fig. 7 compares the TD solution at $t_D = 1000$ (i.e. using a timestep size of 533.35 days) to FD solutions obtained for various space discretizations **Table 3**. To minimize the contribution of time-related truncation error to the FD solutions, a very fine time discretization is used, requiring 543 timesteps and 1117 matrix inversions. With an increasingly fine space discretization, the FD solutions approach the TD solution. The superiority of the TD is obvious, as it is capable of delivering a more accurate solution with a single (or none at all) algebraic equation (which has to be solved N_S times) than a FD scheme which needs to invert 1117 times a matrix of order 111. This reduces the computational effort by orders of magnitude.

In **Fig. 7a** the TD method is compared to FD solutions which use increasingly fine time discretizations. To minimize the effects of space-related truncation errors, a fine space discretization (111 gridblocks) is used. A pattern similar to the one observed in **Fig. 7** is evident: with an increasingly fine time discretization, the FD solutions tend towards the analytical and the TD solutions, further attesting to the power of the method. The TD solution exhibits a very small deviation from the analytical solution, and is consistently superior to the FD solution. The superiority of TD persisted even when a very fine time discretization (263 timesteps, and a total of 541 matrix solutions) was used in the FD simulation. The corresponding TD computational effort to achieve this level of accuracy is essentially trivial: either direct substitution into Eqs. 26 through 29 at the desired time and location, or (in the case of the 2 subdomains of subproblem 1b) solution of the single point algebraic Eq. 21 N_S times, followed by the direct substitution.

Verification and Test Problem 2. Test Problem 2 involves flow in a heterogeneous one-dimensional system composed of five locally homogeneous subdomains. The fluid properties remain as in Problem 1. There are seven wells in the reservoir. The reservoir geometry, dimensions, and properties, as well as the well rates and the well locations, are presented in **Table 4**. A fine spatial discretization was used in the FD simulation because of the number of the wells (7) and the existence of numerous interfaces of different permeability.

The power and flexibility of the TD method is clearly demonstrated in **Fig. 8**, where the variation of the pressure drop (from the initial pressure of 5000) with distance at $t = 200$ days is illustrated. Using a single timestep, the TD solution easily captures the sharp peaks (associated with the presence of wells), as well as the abrupt changes in the pressure profile caused by permeability differences at the interfaces of the various subregions. This is achieved by solving a matrix of order 4 (i.e. the number of unknown internal boundaries) N_S times. For the same effect, the FD simulation requires the solution of the coefficient matrix (of order 178) 447 times (213 timesteps), and needs execution times larger by orders of magnitude.

Verification and Test Problem 3. Test Problem 3 involves two-dimensional flow towards a well at the center of a bounded square reservoir with an infinite conductivity vertical fracture at the center of the square. The fluid properties remain as in Test Problem 1. **Table 5** presents the reservoir properties and dimensions, as well as the grid discretization (a total of 960 gridblocks) used in the FD simulations. **Fig. 9** shows the reservoir geometry and the domain discretization used in the TD method, in which two subdomains (defined by the extent of the vertical fracture and indicated in the schematic) and a single unknown boundary are involved. The well pressure is maintained at 3000 psi. We used the analytical solution of Gringarten *et al*[10] (which predicts the unsteady-state pressure at the well) as a reference.

In **Fig. 10** we compare the TD and analytical solutions at the well at 9 observation times. We let $N_S = 12$ in the TD simulations. We observed a pattern similar to the

one in Test Problem 1. The two solutions coincided regardless of the magnitude of observation time. This testifies to the power and accuracy of the TD method, and confirms the complete insensitivity of the method to the size of the time increment.

Analytical solutions of the pressure distribution in the formation do not exist for this problem. In **Fig. 11** we compare the TD solution to 4 FD solutions along the y axis at $x = 0.025$ ft at t =365 days. We observe the established pattern: with an increasing number of Δt's the FD solutions tend to the TD solution, and, consequently, the difference between the two solutions decreases. Using a very fine time discretization (79 timesteps, and a total of 231 inversions of a matrix of order 960), the FD yielded a solution within 0.1 psi of the TD solution. The corresponding computational requirements of the TD method were minimal: (1) a single equation (Eq. 66) had to be solved $N_T = 200$ times to provide the $\hat{U}_1(n)$, $n = 1, \ldots, N_T$ at the unknown boundary, (2) the process was repeated N_S times, and (3) the solution at the desired locations (x_ℓ, y_ℓ) in the Laplace space was obtained from the accelerated Eq. 76, and (4) the solution at $t = 365$ days was obtained from Eq. 38.

In **Fig. 12** we study the effect of N_S on the performance of TD along the same axis and at the same time by comparing the absolute difference between the TD solutions for different N_S values from a reference, taken as the solution obtained with $N_S = 8$. All solutions (even the one with $N_S = 6$) exhibit extremely small pressure differences from each other, i.e. less than 0.5 psi when p is in excess of 3000 psia. These results confirm our previous observations that the accuracy of TD is virtually insensitive to the value of N_S for $8 \leq N_S \leq 20$.

Conclusions

1. A new numerical method, the Transformational Decomposition (TD) method, was developed for the solution of the nonlinear, parabolic Partial Differential Equation (PDE) of transient, slightly compressible, single-phase liquid flow through porous media.

2. Because TD uses a Laplace transform formulation, it eliminates the need for time discretization and allows an unlimited timestep size without loss of stability or accuracy. By using Finite Cosine Transforms, the method drastically reduces the need for space discretization, requiring only a small number of large subdomains for an accurate solution.

3. The TD method provides semi-analytical solutions in space and time by decomposing the original PDE into a small number of algebraic equations, and equating and solving for conditions at internal boundaries. These solutions are fully differentiable and integrable, allowing the determination of continuous velocity maps and easy mass balance calculations.

4. Three test problems were investigated. With finer space and time discretizations, the FD solutions tend to approach the TD solution. The TD method provides a solution generally more accurate than the FD solution. This was expected because the elimination of the traditional time and space discretizations limit the truncation error.

5. We established that $10 \leq N_S \leq 12$ is sufficient to provide an extremely accurate solution. Although the accuracy increases with increasing N_S for $N_S \leq 20$, the improvement is insufficient to justify the additional execution time.

6. The TD method may significantly reduce the computer memory requirements because discretization in time is not needed, and a very coarse grid suffices for the space discretization.

7. Execution times may be substantially reduced because smaller matrices are inverted in the TD method, and solutions are obtained at the desired points in space and time only, while in standard numerical methods solutions are necessary at all of the points of the discretized time and space domains.

Nomenclature

C_L	=	fluid compressibility
C_R	=	rock compressibility
C_T	=	$\phi\,(1 + C_R/C_L)\,R^{(C_R/C_L)}$
C_β	=	defined in Eq. 21
X_i	=	the length of subdomain$i$ in the x direction
Y_i	=	the length of subdomain$i$ in the y direction
g	=	gravitational acceleration
h	=	formation thickness
k	=	absolute permeability
L	=	length of fracture
p	=	pressure
p_D	=	dimensionless pressure (Eq. 97)
q	=	volumetric flow rate per unit volume
$\tilde{q}$	=	mass flow rate per unit volume
$\ddot{q}$	=	defined in Eq. 7
t	=	time
t_D	=	dimensionless time (Eq. 97)
s	=	Laplace transform parameter
x_i	=	local x coordinate in subdomain i
x_e	=	reservoir half length
x_f	=	fracture half length
x_D	=	dimensionless distance (Eq. 97)
y_i	=	local y coordinate in subdomain i
y_e	=	reservoir half width
z	=	vertical coordinate
z_e	=	elevation
β	=	$1/(formationvolumefactor)$
Δp	=	difference between the TD and the FD solution
Δt	=	timestep
Δt_{max}	=	maximum allowable timestep
$\Delta t_{\Delta pmax}$	=	defined after Eq. 38
$\Delta\Psi$	=	defined in Eq. A-2
λ, η	=	defined after Eq. 3

μ = dynamic viscosity
ρ = fluid density
ϕ = porosity
Ψ = defined in Eq. 7

Acknowledgements

This work was supported by the U.S. Department of Energy under Contract No. DE-AC03-76SF00098. The authors are indebted to Drs. Robert Zimmerman and Karsten Pruess for their valuable help and suggestions.

References

1. Moridis, G.J., and Reddell, D.L.:"Transformational Decomposition (TD) Methods for the Solution of the Groundwater Flow Equation",paper H22G-01 presented at the 1991 AGU Fall Meeting, San Francisco, December 9-13,1991, *EOS Trans. of AGU* (October 1991), **72**, No. 44.
2. Goode, P.A., and Thambynayagam, R.K.:"Pressure Drawdown and Buildup Analysis of Horizontal Wells in Anisotropic Media", *SPE Formation Evaluation* (December 1987) **27**, 683-697.
3. Moridis, G.J., McVay, D.A., Reddell, D.L., and Blasingame, T.A.:"The Laplace Transform Finite Difference (LTFD) Numerical Method for Simulation of Compressible Fluid Flow in Reservoirs", paper SPE 22888 presented at the 1991 66th Annual Technical Conference and Exhibition, Dallas, TX, October 6-9.
4. Sneddon, I.N.:"The Use of Integral Transforms", McGraw-Hill Book Company, New York City (1972), 539.
5. Gradshteyn, I.M, and Ryzhik, I.M.:"Table of Integrals, Series, and Products", Academic Press, Inc., San Diego (1980), 1160.
6. Stehfest, H.: "Numerical Inversion of Laplace Transforms", *Communications of the ACM* (Jan. 1970), **13**, No. 1, Algorithm 368, 47-49.
7. Stehfest, H.: "Numerical Inversion of Laplace Transforms", *Communications of the ACM* (Jan. 1970), **13**, No. 10, Algorithm 368, 56.
8. MacDonald, J.R.:"Accelerated Convergence, Divergence, Iteration, Extrapolation,and Curve Fitting", *Journal of Applied Physics* (October 1964) **35**,10, 3034-3041.
9. *SABRE- A General Purpose Three Dimensional, Three Phase Petroleum Reservoir Simulator, User's Manual*, Version 2.00, S. A. Holditch & Associates, College Station (October 1989).
10. Gringarten, A.C., Ramey, H.J., Jr., ann Raghavan, R.: "Unsteady-State Pressure Distributions Created by a Well with a Single Infinite Conductivity Vertical Fracture, SPEJ (August 1974) 347-360.

SI Metric Conversion Factors

bbl	× 1.589873	E-01 = m^3
cp	× 1.0	E-03 = Pa·s
ft	× 3.048	E-01 = m
md	× 9.869233	E-04 = μm^2
psi	× 6.894757	E+00= kPa

TABLE 1 - TIME DISCRETIZATION FOR THE FD METHOD
(MS: Matrix Solutions)

Test Problem #	Δt_0 (days)	Δt_{max} (days)	M_L	Δp_{max} (psi)	Number of Δt	Number of MS
1	10	30	3	1000	10	30
	0.1	10	3	500	30	78
	0.001	1	3	250	263	541
2	0.001	1	3	200	213	433
3	1	100	5	1000	10	39
	0.1	50	5	500	18	59
	0.01	25	5	500	21	68
	0.01	2	5	250	86	329

TABLE 2 - FLUID PROPERTIES IN TEST PROBLEM 1

p	5000 psi
B	1.0
μ	1 cp
C_L	1.5×10^{-5} psi^{-1}

TABLE 3 - RESERVOIR PROPERTIES, GEOMETRY, AND DISCRETIZATION IN TEST PROBLEM 1

	f = 0.15	C_R = 0.0 psi^{-1}	h = 50 ft
	k = 10 md	L = 300 ft	Q = 50 bbl/D
Discretizations			
1) Dx (in ft):	Dx(i) = 2*Dx(i-1), Dx(0) = 1, max{Dx} = 500, MX(1)=16		
2) Dx (in ft):	Dx(i) = 2*Dx(i-1), Dx(0) = 0.2, max{Dx} = 200, MX(1)=34		
2) Dx (in ft):	Dx(i) = 2*Dx(i-1), Dx(0) = 0.05, max{Dx} = 50, MX(1)=111		

TABLE 4 - RESERVOIR GEOMETRY, PROPERTIES AND DISCRETIZATION IN TEST PROBLEM 2

Dimensions in x,y,z (ft) 5000 x 300 x 50 (ft)

Discretization MX = 178 (Dx's of variable size), MY = 1 (Dy = 300 ft), MZ = 1 (Dz = 50 ft)

Subdomain #	k (md)	f	X (ft)	NO	Q (BPD)	Well position (local, ft)
1	50	0.2	800	2	-30, 20	100, 560
2	20	0.18	1200	3	-20, -20, -20	300, 770, 910
3	8	0.12	1400	1	-25	490
4	6	0.08	800	1	-25	650
5	2	0.07	800	0	-	-

TABLE 5 - RESERVOIR PROPERTIES, GEOMETRY, AND DISCRETIZATION IN TEST PROBLEM 3

	f = 0.15, C_R = 0.0 psi^{-1}	h = 30 ft
	$k_x = k_y$ = 10 md	Q = 50 bbl/D
	k_x along x_f (I=1-26, J=1) = 10^7 md	x_f = 500 ft, $x_e = y_e$ = 1000 ft
Discretization		
MX = 40 Dx (in ft)	0.005,0.02,0.025,0.05,0.25,0.25,0.5,1.5, 2.5,7.5,15,25,25,50,50,50,50,50,50,40, 30,20,15,10,5,2.5,2.5,5,10,15,20,30,40,50,50,50,50,50,50,77.5	
MY = 24 Dy (in ft)	0.001,0.004,0.015,0.03,0.05,0.1,0.3,0.5, 1,3,5,10,20,30,50,80,100,100,100,100, 100,100,100,100	

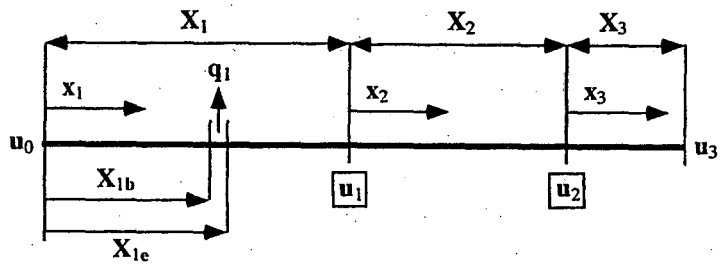

Fig. 1 - The TD method in one dimension. The quantities in the boxes indicate the unknown internal boundaries.

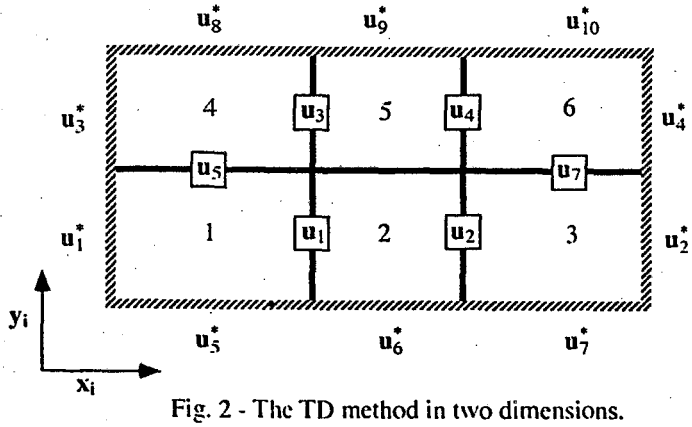

Fig. 2 - The TD method in two dimensions.

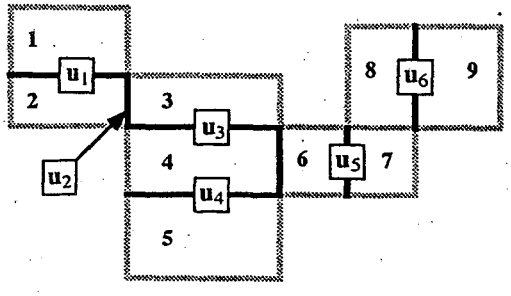

Fig. 3 - The use of the TD method in domains with irregular boundaries.

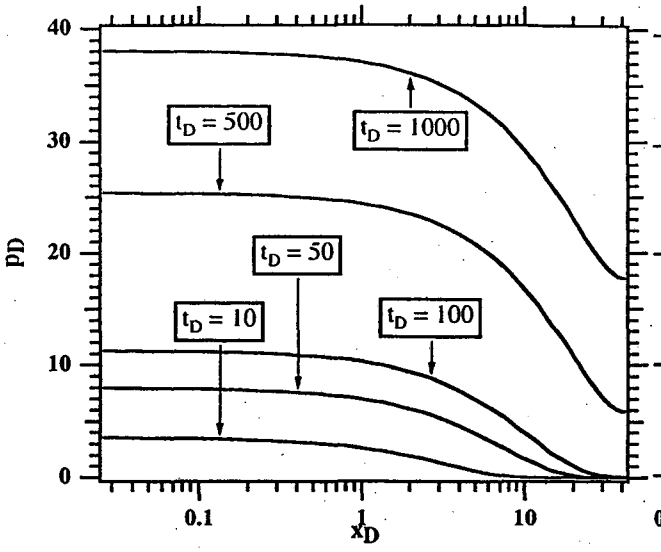

Fig. 4 - Test Problem 1a and 1b. The TDM solutions of p_D for various t_D's.

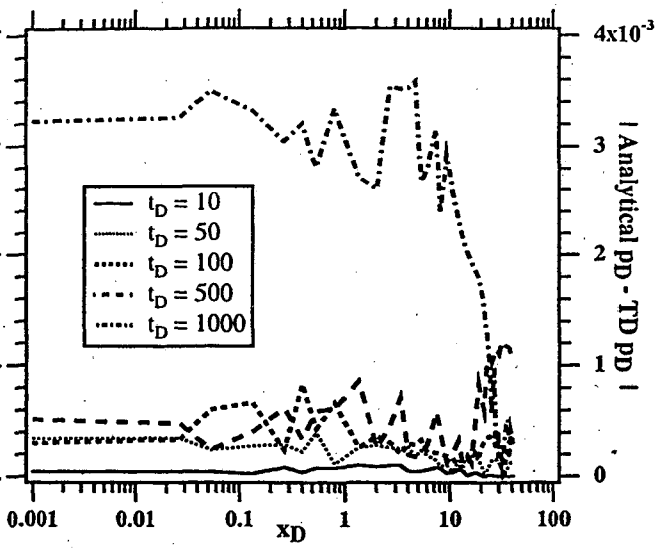

Fig. 5 - Test Problem 1a and 1b. Absolute differences between the TD and the analytical solutions.

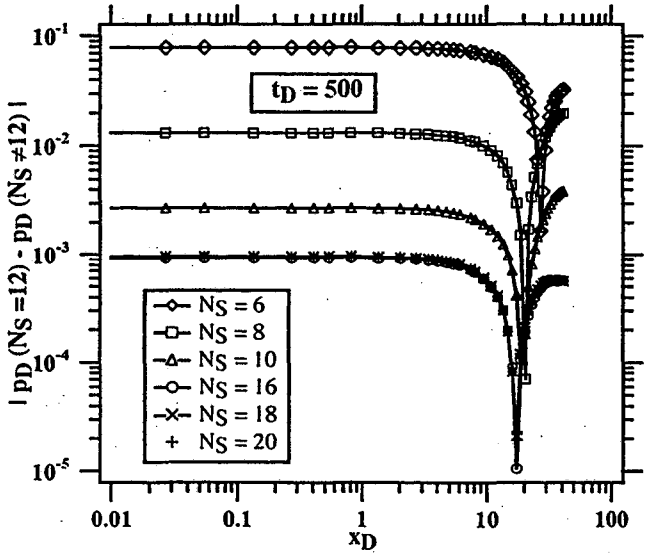

Fig. 6 - Test Problem 1a and 1b. Effect of Ns on the performance of the TD method.

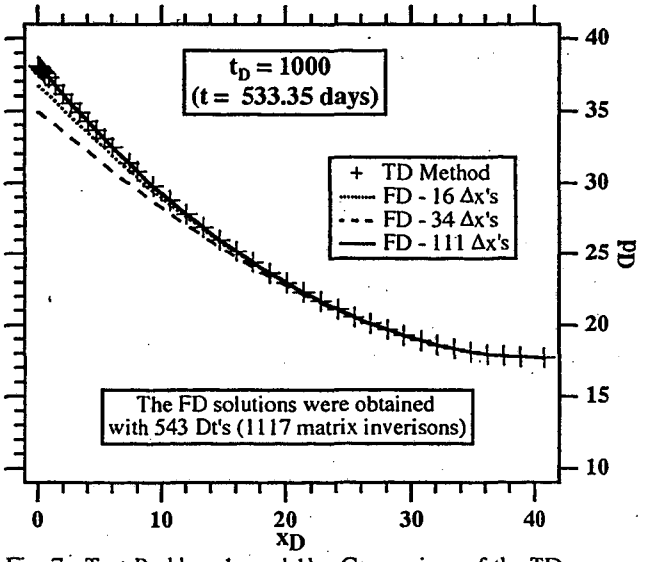

Fig. 7 - Test Problem 1a and 1b. Comparison of the TD to the FD solution with various space discretizations.

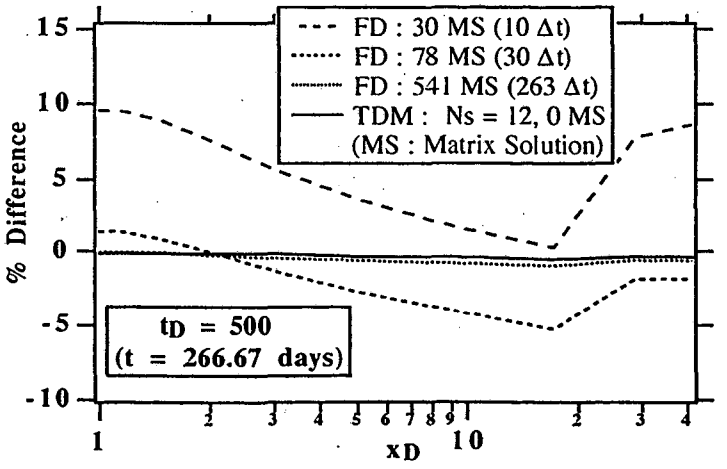

Fig. 7a - Test Problem 1a and 1b. Comparison of the TD solution to the FD solutions with various time discretizations.

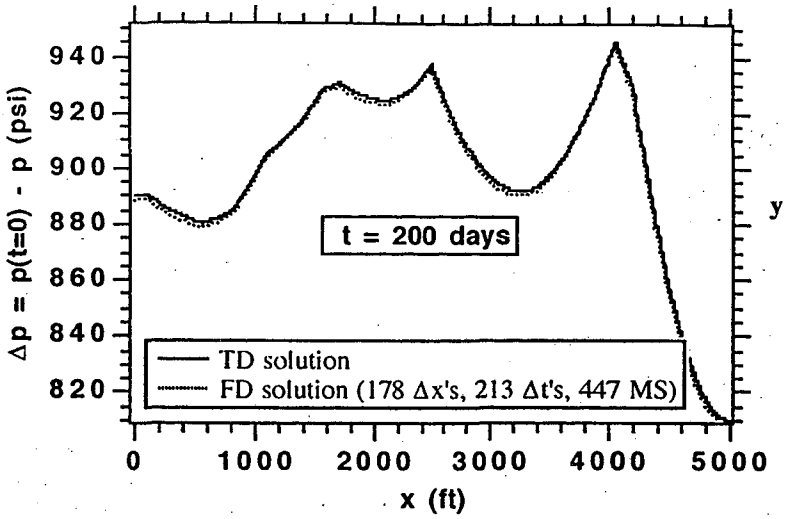

Fig. 8 - Test Problem 2. The TD and the FD solutions.

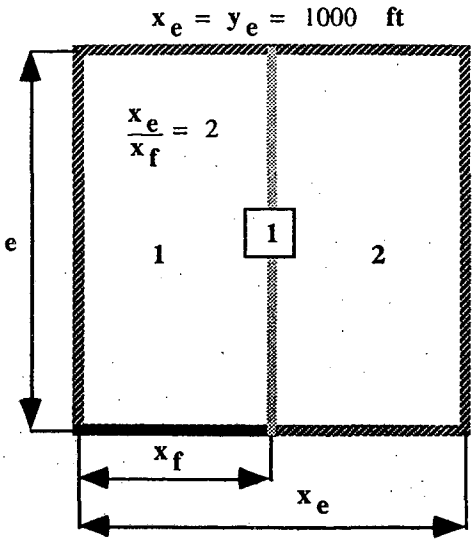

Fig. 9 - Geometry of Test Problem 3. A quarter of the reservoir (shown) was modeled.

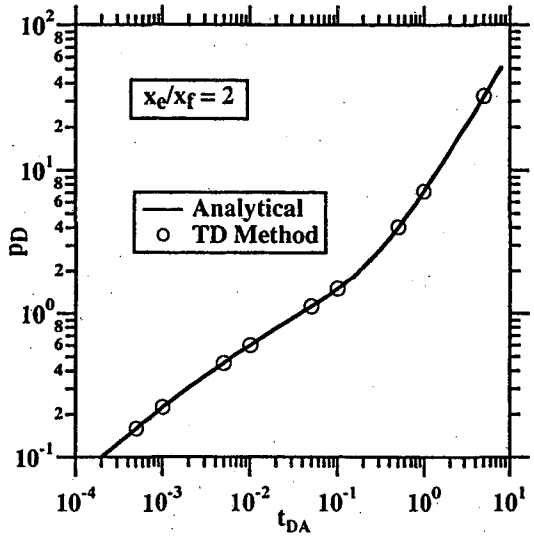

Fig. 10 - Test Problem 3. Comparison of the analytical and the TD solutions.

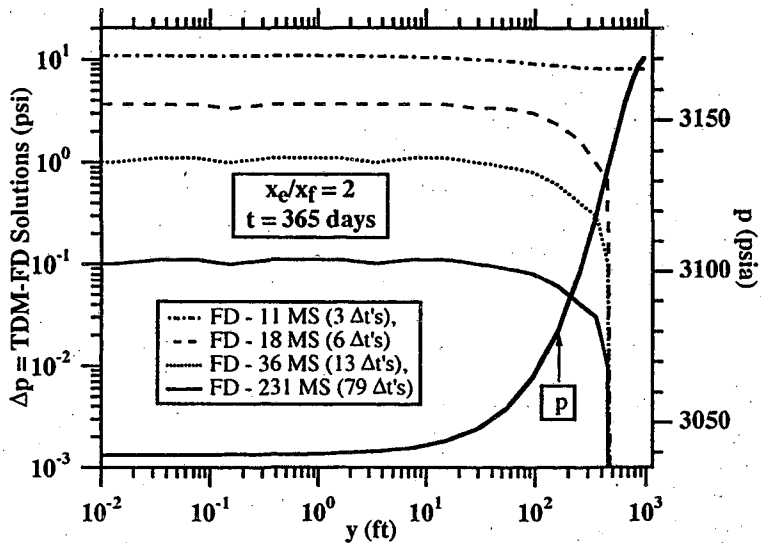

Fig. 11-Test Problem 3. Pressure p and difference Δp between the TD and the FD solutions along y at x=0.025 ft (I=1), t=365 days.

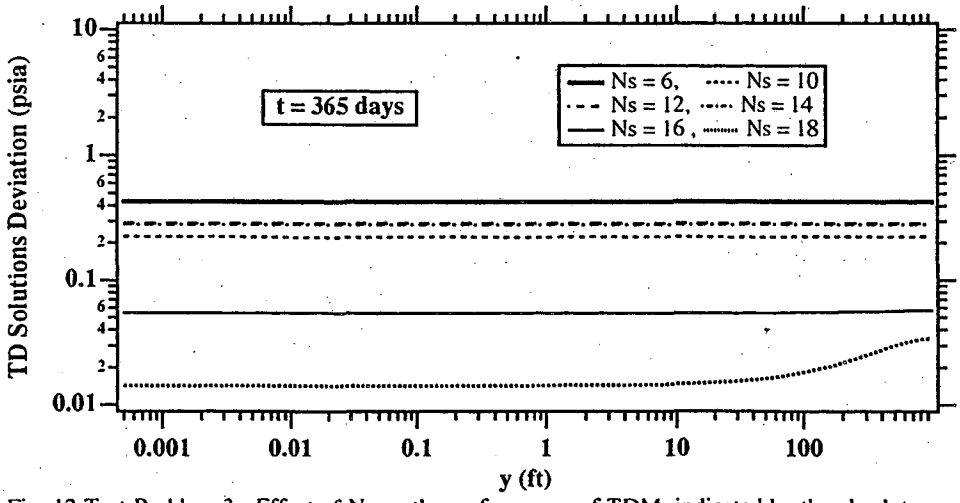

Fig. 12-Test Problem 3. Effect of Ns on the performance of TDM, indicated by the absolute difference of the TDM solutions for Ns = 6,...,18 from the TDM solution for Ns = 8 - Test Problem 2c.

LAWRENCE BERKELEY LABORATORY
UNIVERSITY OF CALIFORNIA
TECHNICAL INFORMATION DEPARTMENT
BERKELEY, CALIFORNIA 94720